Vacancy Ordering and Physical Properties in Defect NaCl-type Solids; M-X (M=Yb, Y, X=S, Se) System

Ji-Yun Lee and Sung-Jin Kim*

Department of Chemistry, Ewha Womans University

Received September 9, 1993

The nonstoichiometric chalcogenides with NaCl-type structure were prepared and the physical and structural properties were studied. The homogeneous range and the structural change were studied based on X-ray powder diffractions using Rietveld-type full-profile fitting technique. Wide homogeneous ranges were observed in Y-S and Y-Se systems, and relatively narrow homogeneous ranges were observed in Yb-S and Yb-Se systems. Both in $Yb_{1-x}S$ and $Yb_{1-x}Se$, a vacancy ordering transition occurred in (111) plane direction. The ordered superstructure had cubic symmetry ($Fm\bar{3}m$) with doubled unit cell "a" parameter compared to the original NaCl-type. The superlattice developed in a continuous second-order transition was characterized by the reduced waved vector $k=(a^*+b^*+c^*)/2$. Y-S system had metallic, and YSe, YbSe systems had semiconducting properties in their homogeneous ranges. It was observed that the change of electronic transport properties in extended homogeneous range did not depend on the relative ratio of metal to nonmetal, but on the quantities of vacancies.

Introduction

The transition metal chalcogenides with NaCl-type structure have been studied for the subjects of much interest because of their interesting properties such as conductivity, magnetic, thermodynamic properties and effectiveness as catalysts. Often, these chalcogenides have been observed to have some range of homogeneity which can be ascribed to vacancies on anion or cation sites, or on both. Furthermore, the vacancies in these solids are observed to order when samples are cooled slowly, and as a result, the symmetry of materials are lowered.[1-10] The understanding of such structural change is important, because such structural changes are frequently associated, directly or indirectly, with interesting and useful properties of materials. For example, the electronic properties of these NaCl-type materials vary from semiconductor to metallic conductor and even to low temperature superconductor in a homogeneous range.[11,12] For the discussion of many interesting properties, it is necessary that the structural phase transitions involving vacancy ordering are to be investigated. Although numerous efforts have been made to explain the nature of vacancy ordering phase transition in defect solids,[13-15] not so many give reliable knowledge concerning these interesting phenomena.

During the investigation of NaCl-type transition metal and rare earth metal chalcogenides, new vacancy ordered phases in Yb-S and Yb-Se were found. The nature of these vacancy ordering phase transition explained based on Landau theory of symmetry and phase transition.[15-19] The electronic properties are studied over the homogeneous ranges in Yb-X and Y-X (X=S, Se) systems.

Experimental

The samples were prepared directly from yttrium or ytterbium metal (99.9% purity from Strem Chem.) and elemental sulfur or selenium (99.999% purity from Strem Chem.). The desired amount of metal and nonmetal (for samples with starting composition in the range (0.5<X/M<1.5) were placed in the outgassed fused sillica tubes which were evaquated, sealed and heated in a tube furnace at about 900 to 1000℃ for 5-7 days. After heating, the samples were ground, pelletized and annealed in the sealed fused silica tubes to achieve homogeneity. For the initial phase analysis of sample, the X-ray powder patterns were taken using θ-2θ diffractometer (Siemens D-500). The diffraction data were taken using stepscan procedure with step size of 0.01-0.02 in 2θ, and for the structure analysis a full-profile pattern fitting Rietveld-type program DBW-PC90 was used.[21] The parameters refined for each diffraction data were scale factor, unit cell parameters, back ground parameters, atomic positions, zero point and overall isotropic thermal parameters.

The electronic resistivities were measured using standard four probe method in which sintered pellets were used and four wire were bound to the sample by indium contacts.

Final compositions of sulfides and selenides were determined by oxidizing them to their highest oxidizing forms in a platinum crucible in air at about 1000℃.

Results and Discussion

The Vacancy Ordering in Yb-X (X=S, Se). The study of the vacancy ordering in defect $Yb_{1-x}X$ (X=S, Se) was undertaken as one of the series of investigations of phase transition in defect NaCl-type solids. The structures of the stoichiometric YbS and YbSe are NaCl-type. The X-ray powder patterns of the samples of different compositions, YbX_x (X=S, Se, x=0.9-1.0), were examined and obtained cell parameters are shown in Figure 1. From the linearity of the cell parameters vs compositions, we concluded that the relatively narrow homogeneous range exists in chalcogen deficient region. In this range, any evidences of vacancy ordering were not observed. However, the metal deficient samples ($Yb_{0.89}Se$ and $Yb_{0.92}S$) cooled slowly from 950℃ to room temperature over several days of period gave evidence of vacancy ordering. These phases with metal deficient site were

*To whom correspondence should be addressed.

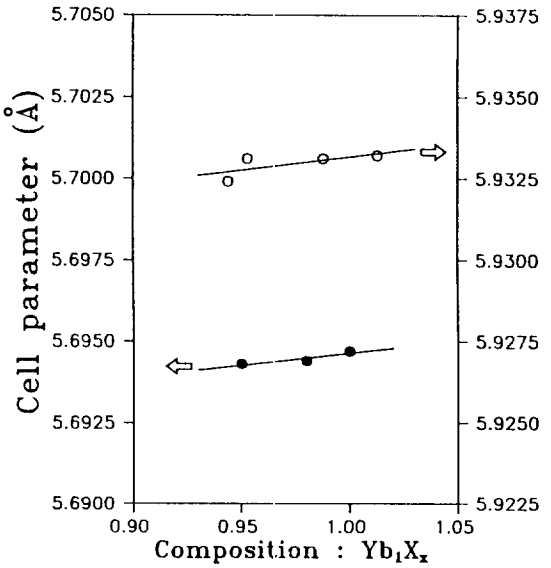

Figure 1. Lattice parameter as a function of composition for $YbSe_x$ (open circle) and YbS_x (closed circle). Sample compositions were taken from combustion analysis.

in common with Sc, Zr, Y, Lu monosulfides and Y monoselenide. It has been reported that $Sc_{1-x}S$, $Zr_{1-x}S$, $Y_{1-x}S$, $Lu_{1-x}S$ and $Y_{1-x}Se$ have high concentrations (upto-25%) of metal vacant site on the parent NaCl-type structure.[1-8]

The powder patterns of $Yb_{0.89}Se$ and $Yb_{0.92}S$ were similar to those of ideal 1 : 1 composition (Yb : S=Yb : Se=1 : 1) except weak extra reflections. The weak reflections could be indexed with twice the NaCl-type "a" parameter, thus the new phase can be considered to have superstructure with broken symmetry (some symmetry elements of NaCl-type structure are lost) resulting from vacancy ordering. Such symmetry breaking transitions occur when a structure changes continuously and these transitions are categorized to be second order.[16-19]

If a structure changes continuously, Landau theory can be applied to solve unknown superstructures. The superstructures are due to the long range ordering of defect sites along particular direction. It is almost impossible to find the way how the defect sites arranged based on geometry alone, but if Landau's four criteria for symmetry breaking transition is applied the number of possible solutions can be greatly reduced.

When the theory was first suggested, Landau used the order parameter η, as a basis for the expansion of the Gibbs free energy:

$$G=G^{\circ}+A\eta^2+C\eta^4$$

Then, the order parameters which minimize the Gibbs free energy are determined, which give the information about symmetries of the solids. In an effort to solve the superstructure, the following four Landau's conditions must be considered: ① The space groups of two crystalline structures related by such a transition must be in a group-subgroup relationship. ② The change of the crystal should correspond to a single irreducible representation of the space group of higher symmetry. ③ In Gibbs free energy expansion, there must be no third-order term of the basis functions invariant under the symmetry operation of the group. ④ For commensurate superstructure, the possible wave vectors to which a second-order transition corresponds must be the high symmetry points of the first Brillouin zone. Since Landau suggested the Landau theory of symmetry and phase transition, Franzen[18] applied and developed the method to characterize the symmetry breaking transition in defect solids.

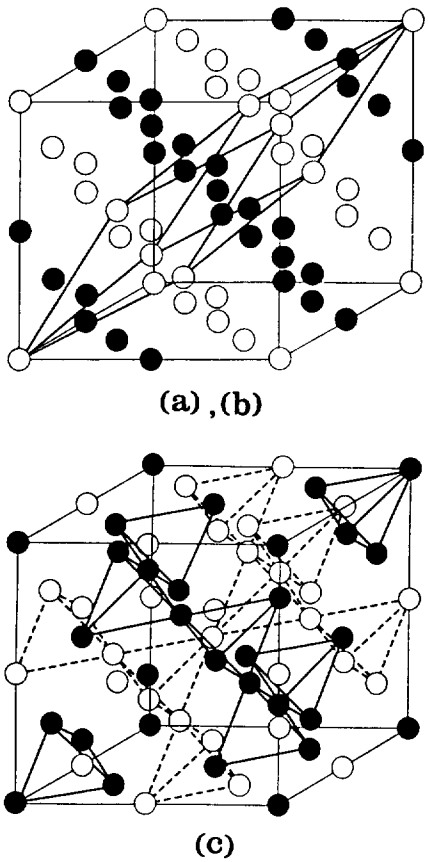

Figure 2. The possible superstructures arising continuously from the NaCl-type. For the clearity only metal positions are shown. a), b) The rhombohedral ($a=(3/2)^{1/2}a_{NaCl}$, $\alpha=\cos^{-1}(5/6)$, R-3m) superstructure observed for $Zr_{1-x}S$ and the cubic superstructure ($a=2a_{NaCl}$, Fm-3m) observed for $Yb_{1-x}Se$ and $Yb_{1-x}S$. c) The cubic superstructure ($a=2a_{NaCl}$, Fd-3m) observed for $Y_{1-x}Se$.

For NaCl-type structure, *T, X, W, L* points in the first Brillouin zone are high symmetry points to be considered according to the fourth condition above. At *L* point, three possible space groups are R-3m, Fm-3m and Fd-3m. The detailed theory and technique are contained in other literatures.[17,18] The possible superstructures arising continuously are shown in Figure 2. For clarity non-metal sites are omitted and only metal sites are shown, and cubic unit cells are doubled in Figure 2(a), (b). The cell inscribed in doubled unit cell (Figure 2(a)) illustrated the rhombohedral unit cell which is a superstructure resulting from metal vacancy ordering in alternate plane along the (111) direction. The closed and open circles indicate the sites with different occupancies. The first solution, R-3m, has been observed in the metal deficient $Sc_{1-x}S$. In these two systems, vacancies are randomly distributed at high temperatures and order in alternate

Table 1. Refined Parameters for $Yb_{0.92}S$ in Fm-3m Space group

Atom	x	y	z	Multiplicity	Occupancy (%)
Yb	0	0	0	4	22.7
Yb	1/2	1/2	1/2	4	98.9
Yb	0	1/4	1/4	24	100.0
Se	1/4	1/4	1/4	8	100.0
Se	1/4	0	0	24	91.1

R=9.3% ($R=100\Sigma|y_i-y_{ci}|/\Sigma|y_i|$, the pattern R-factor, where y_i =observed intensity at i^{th} step, y_{ci}=calculated intensity at i^{th} step.), $a_{super}=2a_{sub}=11.281(2)$ Å.

Table 2. Refined Parameters for $Yb_{0.89}Se$ in Fm-3m Space group

Atom	x	y	z	Multiplicity	Occupancy (%)
Yb	0	0	0	4	11.2
Yb	1/2	1/2	1/2	4	94.5
Yb	0	1/4	1/4	24	94.4
Se	1/4	1/4	1/4	8	76.8
Se	1/4	0	0	24	100.0

R=13.4%, $a_{super}=2a_{sub}=11.740(2)$ Å.

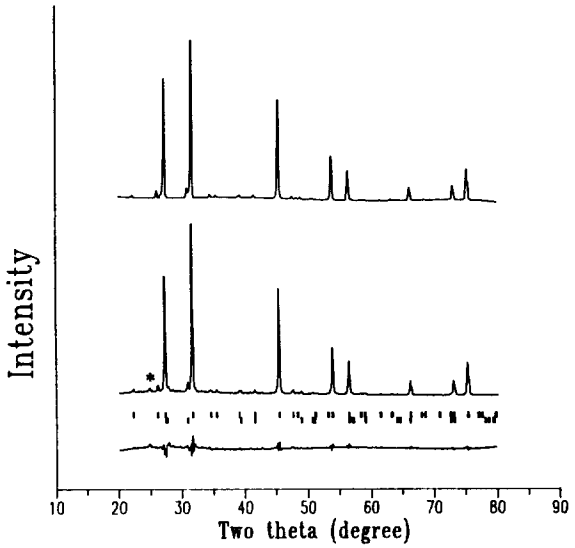

Figure 3. Comparison of calculated (top) and observed (bottom) powder diffraction for $Yb_{0.92}S$. The diffraction peaks at asterisk is the strongist peak of Yb_2S_3 phase. The first set of vertical strokes indicate calculated Bragg peak positions for $Y_{0.89}S$ and the second set for Y_2O_2S phase.

(111) planes when samples are cooled slowly (rhombohedral cell in Figure 2(b)). The third solution, Fd-3m has been found in $Y_{1-x}Se$, and in this system, vacancies order as shown in Figure 2(b). For the first solution, one C_3 symmetry among four C_3 symmetries ($C_{3(x+y+z)}$, $C_{3(-x+y+z)}$, $C_{3(x-y+z)}$, $C_{3(x+y-z)}$) is retained and other three C_3 symmetries are lost. For second (as shown in Figure 2(a)) and third solutions, four C_3 symmetries are retained, but some translation symmetries such as **a**, **b**, **c**, are lost.

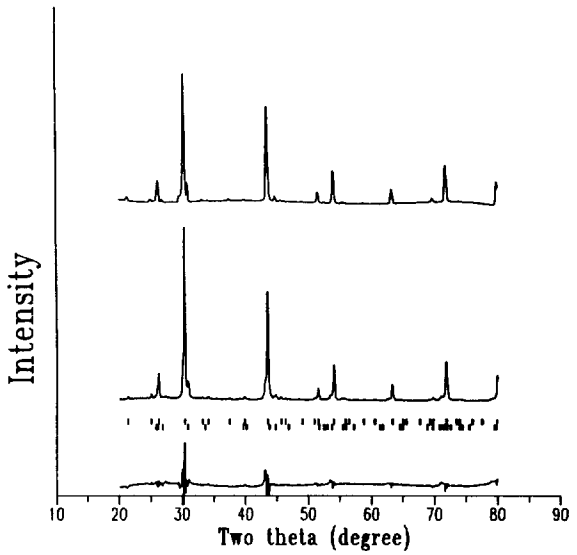

Figure 4. Comparison of calculated (top) and observed (bottom) powder diffraction for $Yb_{0.89}Se$. The first set of vertical strokes indicate calculated Bragg peak positions for $Y_{0.82}Se$ and the second set for Yb_2Se_3 phase.

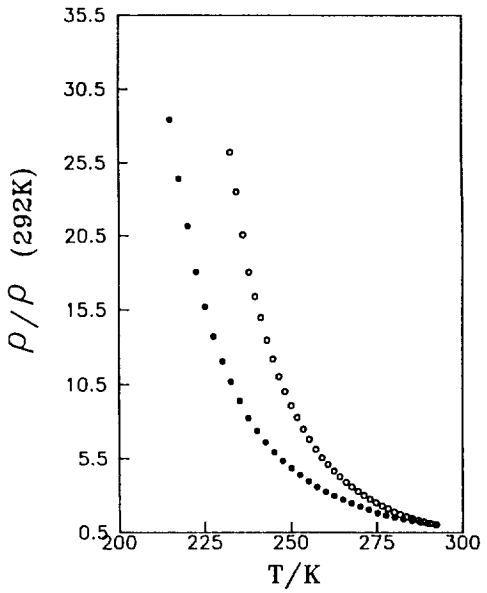

Figure 5. Resistivity as a function of temperature for $Yb_{0.89}Se$ and $Yb_{0.92}S$. Resistivity is normalized to 1 at 292 K.

In our research, we found that the defect sites on ytterbium in $Yb_{0.92}S$ and $Yb_{0.89}Se$ ordered to (111) plane direction with a doubled unit cell. The space group of the superstructure was Fm-3m. This superstructure solution was fitted well to the observed X-ray pattern (Tables 1, 2, Figure 3, 4). This observed superstructure was consistent with Landau theory and these materials were the first example of the metal defect solids with symmetry breaking transition among NaCl-type lanthanide chalcogenides. Additional high temperature X-ray work is required to determine the exact temperature at which the transition occurs from NaCl-type substructure to superstructure.

The results of resistivity measurement suggested that

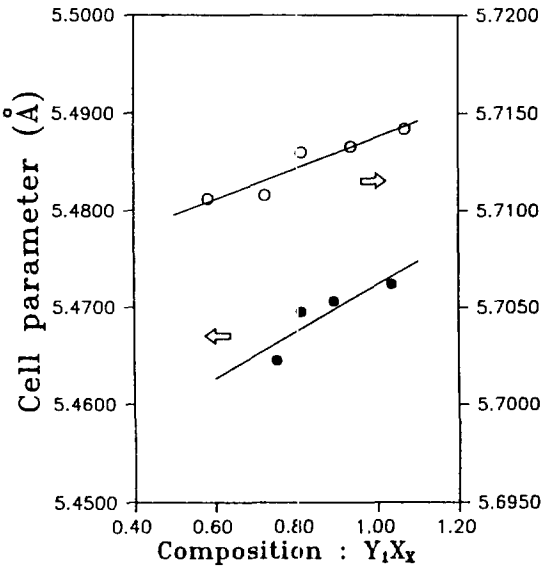

Figure 6. Lattice Parameter as a function of composition for YSe_x (open circle) and YS_x (closed circle). Sample compositions were taken from combustion analysis.

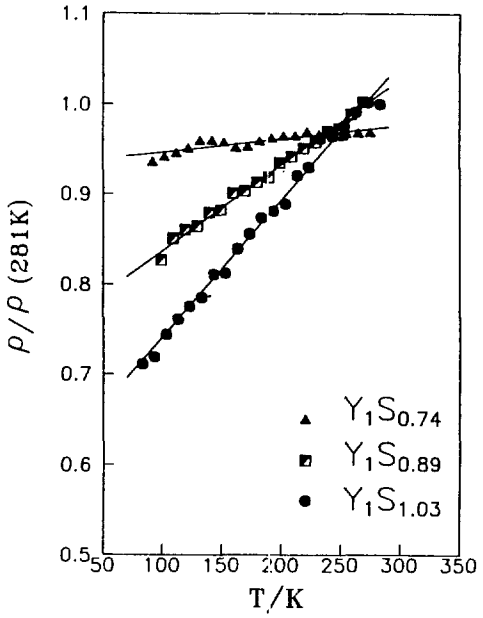

Figure 7. Resistivity as a function of temperature for $Y_{1-x}S$. Resistivity is normalized to 1 at 281 K.

these materials were semiconductor and band gaps were 0.23 and 0.32 eV for YbS and YbS, respectively (Figure 5). The band gap of YbSe was greater than that of YbS and this may be due to the difference in covalency of metal-nonmetal bond. Because the bonds in YbSe are more covalent than those in YbS, the band near the Fermi level is expected to be more dispersive and the band gap might be greater in YbSe.

The Defect Chemistry in YS and YSe. It has been reported that the vacancies in defect yttrium monoselenides order at lower temperature (275± 25℃),[4] and this ordering corresponds to the *L* point of the first Brillouin zone. As in the case of $Yb_{1-x}X$ (S, Se), the ordering corresponds to

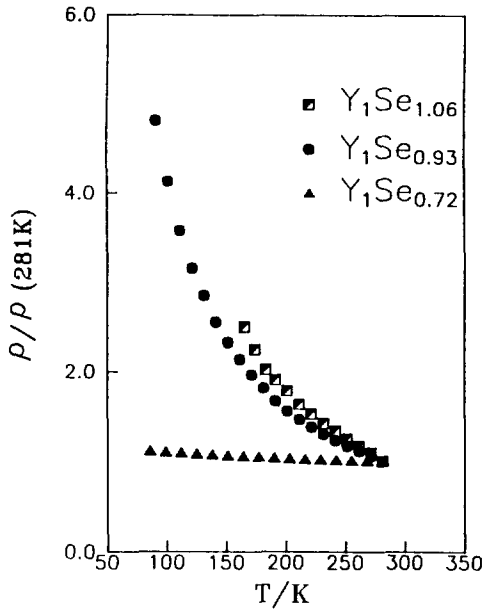

Figure 8. Resistivity as a function of temperature for $Y_{1-x}Se$. Resistivity is normalized to 1 at 281 K.

a combination of all four equivalent k vectors $((a^*+b^*+c^*)/2$, $(-a^*+b^*+c^*)/2$, $(a^*-b^*+c^*)/2$, $(a^*+b^*-c^*)/2)$ in $Y_{1-x}Se$. However, the order parameters in Yb_{1-x} and $Y_{1-x}S$ are different as illustrated in Figures 2(a) and (b).

In this research, a wide homogeneous range in sulfur deficient region was found in Y-S system. Y_5S_7 and NaCl-type structures exist in metal deficient range. The cell parameters changed linearly in $0.72<S/Y<1.06$ range (Figure 6(a)) and this result indicated that the material retained the NaCl structure with 20% defect in sulfur. The electric resistivities were measured for various compositions in homegeneous range. The resistivities vs temperatures were normalized to the value at 281 K. The electronic properties of YS_{1-x} were metallic conductor. It was observed that material became to a poor conductor when x increases (Figure 7), even the relative quantity of metal was increased. This result indicates that the change of electron transport properties in extended homogeneous range does not depend on relative quantities of metal and nonmetal, but depend on absolute quantities of vacancies.

A wide homogeneous range in selenium deficient region was found in Y-Se system (Figure 6(b)). The electrical properties were semiconducting and the band gaps were 0.035, 0.027, 0.003 eV for $YSe_{1.06}$, $YSe_{0.93}$, $YSe_{0.73}$, respectively (Figure 8). When the concentration of defect sites on selenium increased, the band gap decreased.

In summary, we found a new superstructure in YbS and YbSe systems. The new superstructure has a doubled perodicity in a, b, c directions and the space group was Fm-3m. The superstructure was consistent with Landau's condition for second order phase transition. This system is the first example of metal deficient material with such transition among NaCl-type lanthanide chalcogenides.

A wide homogeneous range in sulfur deficient region was found in Y-S and Y-Se systems. The change of electronic transport properties in extended homogeneous range does not depend on relative quantities of metal and nonmetal,

$$MeSi(SiMe_3)_3 \xrightarrow{h\nu} Me\text{-}\ddot{S}i\text{-}SiMe_3 + Me_3SiSiMe_3 \text{ (major pathway)}$$

I II

$$\rightarrow :SiMe_2 + Me_2Si(SiMe_3)_2 \text{ (minor pathway)}$$

$$\rightarrow (Me_3Si)_2MeSi\cdot + \cdot SiMe_3 \text{ (minor pathway)}$$

III

Scheme 1.

lanes.[5-9] Photoproduced silyl radical has directly been detected by EPR spectroscopy.[8,9]

So far, however, clear evidence for the photochemical generation of the silylenes and silyl radicals from I has not been presented in the literature, to our knowledge.

We have studied the photochemical behaviors of I upon UV (mostly, 254 nm) irradiation and the reactivities of photofragments such as silylene and silyl radicals etc.. By employing the appropriate trapping agents, we were able to trap the silylene and silyl radical and to isolate all observed products, and to obtain their unambiguous spectral data including ^{1}H-NMR and mass spectra.

Trapping studies could provide information about the photoinduced decomposition pattern and the photodissociation efficiencies of permethylated oligosilanes. Labelling experiment employing CH_3OD also helps to identify the intermediate species, especially, silyl radical III involved in the photodissociation of I.

In an attempt to estimate the energetics of various reactions observed here, we have performed semiempirical calculations using the PM3 method[12,13] on the thermochemical values of the reactive species and stable products observed or inferred. Only the PM3 results are reported here since in this system, the PM3 calculation is found to be superior to the AM1 calculation.[14,15] The PM3 calculation is quite useful to infer the electronic and vibrational states of the silicon species involved in this study.

Table 1. Thermochemical values derived by the PM3 semiempirical method

Silicon Species	ΔH_f° (kcal/mol) PM3	Experiment
$MeSi(SiMe_3)_3$	−152.6	
$Me_3SiSiMe_3$	−83.2	−87.0± 2.1[a]
$Me\text{-}\ddot{S}i\text{-}SiMe_3$	0.4	
$:SiMe_2$	26.6	26[b]
$Me_2Si(SiMe_3)_2$	−116.7	
$MeHSi(OMe)SiMe_3$	−124.9	
$\cdot SiMe_3$	−15.0	−11.7± 2.4[c]
$\cdot SiMe(SiMe_3)_2$	−71.9	
$MeHSi(SiMe_3)_2$	−99.8	
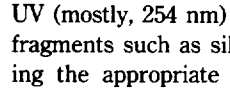	−68.8	
$[Me(Me_3Si)HSi]_2O$	−206.3	
Me_4Si		−54.1± 1.1[c], −55.4[b]
$\cdot OCH_3$	−6.8	−0.5[d]
CH_3OCH_3	−48.3	−44.0[e]
CH_3OH	−51.9	−48.1[e]
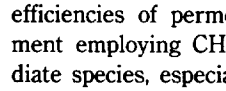	22.2	18.10± 0.24[e]
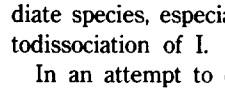	56.2	

[a] J. B. Pedley and J. Rylance, Sussex-N. P. L. Computer analyzed thermochemical data: Organic and organometallic compounds, University of Sussex, 1977. [b] R. Walsh, *Acc. Chem. Res.* 14, [1981], 246. [c] L. Szepes and T. Baer, *J. Am. Chem. Soc.* 106, [1984], 273. [d] J. L. Franklin, J. G. Dillard, H. M. Rosenstock, J. T. Herron, K. Draxl, and F. H. Field, Natl. Stand. Ref. Data Ser., Natl. Bur. Stand., No. 26 (1969). [e] J. O. Cox and G. Pilcher, Thermochemistry of Organic and Organometallic Compounds, Academic Press, New York, 1970.

Experimental

General Data. ^{1}N-NMR spectra were recorded on a Bruker AC-80 FT spectrometer. Gas chromatograph-mass spectra (GC-MS) were recorded on a Shimadzu GCMS-QP 1000, and/or on a Hewlett Packard GC/MS spectrometer consisting of a HP 890 series II gas chromatograph and a HP 5970 series mass selective detector (MSD) operating at an ionization voltage of 70 eV. Flame ionization detector (FID) and thermal conductivity detector (TCD) instruments were employed for analytical gas chromatography. The FID instrument was Varian model 3300. The TCD gas chromatograph was Gow-Mac Series 30. The TCD instrument was also used routinely for separation of reaction mixtures and yield determinations. Yields were based on the amount of unrecovered starting precursor I and were determined with the use of I as an external standard. Chromatographic response factors in the TCD instrument were determined for isolated products or for hydrocarbons with the similar molecular weight as the observed products. All the products were separated by using a 13 ft×1/4″ 20% OV-17 on chromorsorb WHP, 105℃.[16]

Materials. Preparation of $(Me_3Si)_3SiCH_3$: synthesized by the method of Barton.[17] This compound is identified from ^{1}H-NMR, mass, IR, Raman, and UV spectra. ^{1}H-NMR ($CDCl_3$): δ-0.083 (s, 3H, $SiCH_3$), −0.045 (s, 27H, $Si(CH_3)_3$). Mass (70 eV) m/z (relative intensity): M^+ 262 (13), 247 (9), 189 (16), 174 (48), 159 (22), 131 (19), 116 (3.9), 101 (3.4), 73 (100), 59 (10), 45 (23), 43 (8.9). FT-IR (cm^{-1}) (relative intensity): 2951.1 (vs), 2893.2 (s), 2816.1 (w), 1427.3 (m), 1400.3 (m), 1249.9 (vs), 837.1 (vs), 783.1 (vs), 740.7 (m), 690.5 (s), 621.1 (s), 486.1 (s). Raman (cm^{-1}) (relative intensity): 2944 (vs), 2886 (vs), 1430 (vw), 1400 (w), 1254 (w), 1234 (m). 862 (w), 832 (w), 736 (m), 678 (s), 656 (s), 612 (vs), 444 (m), 344 (w), 262 (w), 216 (m), 168 (vs). UV absorptions in a 5×10^{-4} M cyclohexane solution: λ_{max}=230 nm, 277 nm.

Neat photolysis of $MeSi(SiMe_3)_3$. 2.0 g (7.6 mmol) of I and 5 ml of cyclohexane were placed in a cylindrical quartz vessel (o.d. 21 mm, length 340 mm). The reaction mixture was thoroughly degassed three times by the freeze-pump-thaw method. The quartz tube was placed in a Rayonet reactor. The samples was irradiated for 70 hr by medium-pressure mercury lamps. 28% of the starting material was consumed. The excess solvent was removed by a simple distillation. Final purification of the products was achieved by gas chromatography. The stable products obtained were $Me_3SiSiMe_3$

$$MeSi(SiMe_3)_3 \xrightarrow{h\nu} Me\text{-}\ddot{S}i\text{-}SiMe_3 + Me_3SiSiMe_3 \text{ (major pathway)}$$

I II

$$\rightarrow :SiMe_2 + Me_2Si(SiMe_3)_2 \text{ (minor pathway)}$$

$$\rightarrow (Me_3Si)_2MeSi\cdot + \cdot SiMe_3 \text{ (minor pathway)}$$

III

Scheme 1.

lanes.[5-9] Photoproduced silyl radical has directly been detected by EPR spectroscopy.[8,9]

So far, however, clear evidence for the photochemical generation of the silylenes and silyl radicals from I has not been presented in the literature, to our knowledge.

We have studied the photochemical behaviors of I upon UV (mostly, 254 nm) irradiation and the reactivities of photofragments such as silylene and silyl radicals etc.. By employing the appropriate trapping agents, we were able to trap the silylene and silyl radical and to isolate all observed products, and to obtain their unambiguous spectral data including ^{1}H-NMR and mass spectra.

Trapping studies could provide information about the photoinduced decomposition pattern and the photodissociation efficiencies of permethylated oligosilanes. Labelling experiment employing CH_3OD also helps to identify the intermediate species, especially, silyl radical III involved in the photodissociation of I.

In an attempt to estimate the energetics of various reactions observed here, we have performed semiempirical calculations using the PM3 method[12,13] on the thermochemical values of the reactive species and stable products observed or inferred. Only the PM3 results are reported here since in this system, the PM3 calculation is found to be superior to the AM1 calculation.[14,15] The PM3 calculation is quite useful to infer the electronic and vibrational states of the silicon species involved in this study.

Table 1. Thermochemical values derived by the PM3 semiempirical method

Silicon Species	ΔH_f° (kcal/mol) PM3	Experiment
$MeSi(SiMe_3)_3$	−152.6	
$Me_3SiSiMe_3$	−83.2	−87.0± 2.1[a]
$Me\text{-}\ddot{S}i\text{-}SiMe_3$	0.4	
$:SiMe_2$	26.6	26[b]
$Me_2Si(SiMe_3)_2$	−116.7	
$MeHSi(OMe)SiMe_3$	−124.9	
$\cdot SiMe_3$	−15.0	−11.7± 2.4[c]
$\cdot SiMe(SiMe_3)_2$	−71.9	
$MeHSi(SiMe_3)_2$	−99.8	
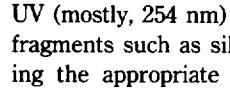	−68.8	
$[Me(Me_3Si)HSi]_2O$	−206.3	
Me_4Si		−54.1± 1.1[c], −55.4[b]
$\cdot OCH_3$	−6.8	−0.5[d]
CH_3OCH_3	−48.3	−44.0[e]
CH_3OH	−51.9	−48.1[e]
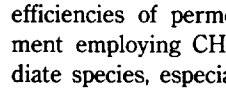	22.2	18.10± 0.24[e]
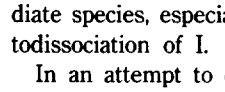	56.2	

[a] J. B. Pedley and J. Rylance, Sussex-N. P. L. Computer analyzed thermochemical data: Organic and organometallic compounds, University of Sussex, 1977. [b] R. Walsh, *Acc. Chem. Res.* 14, [1981], 246. [c] L. Szepes and T. Baer, *J. Am. Chem. Soc.* 106, [1984], 273. [d] J. L. Franklin, J. G. Dillard, H. M. Rosenstock, J. T. Herron, K. Draxl, and F. H. Field, Natl. Stand. Ref. Data Ser., Natl. Bur. Stand., No. 26 (1969). [e] J. O. Cox and G. Pilcher, Thermochemistry of Organic and Organometallic Compounds, Academic Press, New York, 1970.

Experimental

General Data. ^{1}N-NMR spectra were recorded on a Bruker AC-80 FT spectrometer. Gas chromatograph-mass spectra (GC-MS) were recorded on a Shimadzu GCMS-QP 1000, and/or on a Hewlett Packard GC/MS spectrometer consisting of a HP 890 series II gas chromatograph and a HP 5970 series mass selective detector (MSD) operating at an ionization voltage of 70 eV. Flame ionization detector (FID) and thermal conductivity detector (TCD) instruments were employed for analytical gas chromatography. The FID instrument was Varian model 3300. The TCD gas chromatograph was Gow-Mac Series 30. The TCD instrument was also used routinely for separation of reaction mixtures and yield determinations. Yields were based on the amount of unrecovered starting precursor I and were determined with the use of I as an external standard. Chromatographic response factors in the TCD instrument were determined for isolated products or for hydrocarbons with the similar molecular weight as the observed products. All the products were separated by using a 13 ft×1/4″ 20% OV-17 on chromorsorb WHP, 105℃.[16]

Materials. Preparation of $(Me_3Si)_3SiCH_3$: synthesized by the method of Barton.[17] This compound is identified from ^{1}H-NMR, mass, IR, Raman, and UV spectra. ^{1}H-NMR ($CDCl_3$): δ-0.083 (s, 3H, $SiCH_3$), −0.045 (s, 27H, $Si(CH_3)_3$). Mass (70 eV) m/z (relative intensity): M^+ 262 (13), 247 (9), 189 (16), 174 (48), 159 (22), 131 (19), 116 (3.9), 101 (3.4), 73 (100), 59 (10), 45 (23), 43 (8.9). FT-IR (cm^{-1}) (relative intensity): 2951.1 (vs), 2893.2 (s), 2816.1 (w), 1427.3 (m), 1400.3 (m), 1249.9 (vs), 837.1 (vs), 783.1 (vs), 740.7 (m), 690.5 (s), 621.1 (s), 486.1 (s). Raman (cm^{-1}) (relative intensity): 2944 (vs), 2886 (vs), 1430 (vw), 1400 (w), 1254 (w), 1234 (m). 862 (w), 832 (w), 736 (m), 678 (s), 656 (s), 612 (vs), 444 (m), 344 (w), 262 (w), 216 (m), 168 (vs). UV absorptions in a 5×10^{-4} M cyclohexane solution: λ_{max}=230 nm, 277 nm.

Neat photolysis of $MeSi(SiMe_3)_3$. 2.0 g (7.6 mmol) of I and 5 ml of cyclohexane were placed in a cylindrical quartz vessel (o.d. 21 mm, length 340 mm). The reaction mixture was thoroughly degassed three times by the freeze-pump-thaw method. The quartz tube was placed in a Rayonet reactor. The samples was irradiated for 70 hr by medium-pressure mercury lamps. 28% of the starting material was consumed. The excess solvent was removed by a simple distillation. Final purification of the products was achieved by gas chromatography. The stable products obtained were $Me_3SiSiMe_3$

Table 2. ^{1}H-NMR[a] and mass[b] spectral data for the products

$Me_3SiSiMe_3$	Mass: M^+ 146 (10), 131 (22), 115 (1.8), 73 (100), 59 (3.4), 45 (17), 43 (9.4), 32 (3.4).
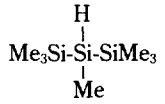	^{1}H-NMR (C_6D_6): δ 0.03 (s, 18H, $Si(CH_3)_3$), 0.30 (d, 3H, J=5.0 Hz, $SiCH_3$), 3.25 (q, 1H, J=5.0 Hz, SiH); mass: M^+ 190 (12), 175 (10), 131 (5.8), 116 (28), 115 (6.6), 102 (27), 101 (19), 73 (100), 59 (13), 45 (24), 43 (14), 32 (18).
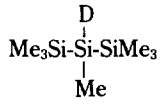	^{1}H-NMR (C_6D_6): δ 0.16 (s, 18H, $SiCH_3)_3$), 0.41 (s, 3H, $SiCH_3$); mass: M^+ 191 (6.8), 176 (11), 131 (4.1), 116 (32), 103 (32), 102 (10), 101 (19), 85 (2.4), 73 (100), 60 (7.1), 59 (9.0), 45 (28), 43 (17).
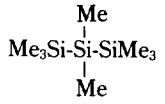	^{1}H-NMR (C_6D_6): δ 0.19 (s, 18H, $Si(CH_3)_3$), 0.66 (s, 6H, $SiCH_3$); mass: M^+ 204 (14), 189 (10), 145 (1.9), 131 (62), 116 (35), 115 (9.8), 101 (8.3), 99 (2.3), 73 (100), 59 (94), 45 (30), 43 (13).
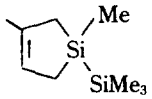 (IV)	^{1}H-NMR (C_6D_6): 0.07 (s, 9H, $Si(CH_3)_3$), 0.14 (s, 3H, $SiCH_3$), 1.39 (s, 3H, CCH_3), 1.62 (s, 2H, CH_2), 1.77 (d, 2H, CH_2), 5.02 (m, 1H CH=C); mass: M^+ 184 (15), 169 (100), 141 (11), 111 (42), 110 (24), 109 (29), 101 (16), 95 (13), 73 (97), 69 (7), 59 (24), 45 (33), 43 (37).
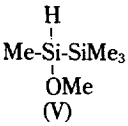 (V)	^{1}H-NMR (C_6D_6): δ 0.16 (s, 18H, $Si(CH_3)_3$), 0.12 (d, 3H, J=3.9 Hz, $SiCH_3$), 3.38 (s, 3H, OCH_3), 5.24 (q, 1H, J=3.9 Hz, SiH); mass: M^+ 148 (5.6), 147 (15), 133 (96), 117 (11), 103 (15), 89 (13), 73 (100), 59 (97), 45 (47) 44 (7), 43 (25), 32 (13), 31 (6.0).
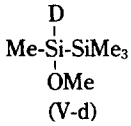 (V-d)	^{1}H-NMR (C_6D_6): δ 0.16 (s, 9H, $Si(CH_3)_3$), 0.12 (s, 3H, $SiCH_3$), 3.38 (s, 3H, OCH_3); mass: M^+ 149 (4.7), 148 (13), 134 (93), 118 (6.0), 117 (3.8), 104 (14), 103 (5.6), 89 (11), 76 (10), 74 (23), 73 (100), 60 (27), 59 (70), 46 (18), 45 (36), 43 (25), 32 (5.6), 31 (5.6).
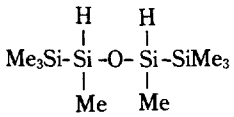 (VI)	^{1}H-NMR (C_6D_6): 0.10 (s, 18H, $Si(CH_3)_3$), 0.30 (d, 6H, J=3.9 Hz, $SiCH_3$), 5.20 (q, 2H, J=3.9 Hz, SiH); mass: M^+ 250 (1.0), 235 (5.6), 205 (32), 176 (15), 161 (22), 147 (8.4), 133 (14), 117 (69), 103 (20), 73 (100), 59 (22), 45 (34), 43 (15).
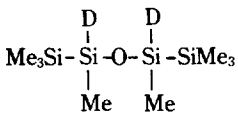 (VI-d_2)	^{1}H-NMR (C_6D_6): 0.13 (s, 18H, $Si(CH_3)_3$), 0.42 (s, 6H, $SiCH_3$); mass: M^+ 252 (1.9), 237 (9.4), 205 (48), 179 (13), 177 (20), 162 (21), 147 (8.5), 134 (16), 117 (76), 104 (20), 73 (100), 60 (19), 59 (6.6), 45 (32), 43 (13), 32 (9.4).
Et_3SiSiH_2Me	^{1}H-NMR (C_6D_6): 0.13 (t, 3H, J=5.1 Hz, $SiCH_3$), 0.57 (m, 6H, $SiCH_2$), 0.97 (m, 9H, CCH_3), 3.71 (q, 2H, J=5.1 Hz, SiH_2); mass: M^+ 160 (14), 131 (10), 115 (100), 103 (27), 87 (94), 75 (14), 73 (7.1), 59 (28), 45 (7.1), 43 (7.1).
$Et_3SiSiHMe_2$	Mass: M^+ 174 (31), 145 (13), 117 (31), 115 (100), 103 (7.1), 89 (29), 87 (94), 73 (7.1), 59 (28), 45 (7.1), 43 (7.1).
$Me_3SiSiEt_3$	^{1}H-NMR (C_6D_6): 0.15 (s, 9H, $SiCH_3$), 0.57 (m, 6H, $SiCH_2$), 0.99 (m, 9H, CCH_3); mass: M^+ 188 (56), 173 (11), 159 (34), 145 (10), 131 (53), 115 (93), 103 (49), 87 (100), 73 (36), 59 (36), 45 (13), 43 (7.1).
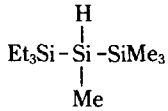	^{1}H-NMR (C_6D_6): 0.20 (s, 9H, $SiCH_3$), 0.20 (d, 3H, J=5.3 Hz, $SiCH_3$), 0.64 (m, 6H, $SiCH_2$), 1.01 (m, 9H, CCH_3), 3.46 (q, 1H, J=5.3 Hz, SiH); mass: M^+ 232 (52), 217 (15), 203 (16), 189 (8.1), 175 (16), 158 (39), 147 (27), 130 (41), 115 (80), 102 (100), 87 (95), 73 (44), 59 (35), 45 (12), 43 (6.7).
$Et_3SiSiEt_3$	Mass: M^+ 230 (54), 201 (56), 173 (46), 145 (38), 115 (100), 87 (87), 59 (37).

[a] 80 MHz. [b] (70 eV) m/z (relative intensity).

(50%) and $(Me_3Si)_2SiMe_2$ (8.7%). All these products were identified by ^{1}H-NMR and mass spectroscopy. The NMR and mass spectroscopic data are given in Table 2.

Photolysis of $MeSi(SiMe_3)_3$ in the presence of 2-methyl-1,3-butadiene. 1.0 g (3.8 mmol) of I, 0.26 g (7.6 mmol) of 2-methyl-1,3-butadiene and 5 m*l* of cyclohexane were placed in the cylindrical quartz vessel. The reaction mixture was thoroughly degassed three times by the freeze-pump-thaw method. The sample was irradiated for 60 hr by medium-pressure mercury lamps. 47% of the starting material was consumed. The excess solvent was removed by a simple distillation. Final purification of the products was achieved by gas chromatography (the same column and temperature for the neat photolysis system). The products obtained were Me_3Si-$SiMe_3$ (77%), $(Me_3Si)_2SiHMe$ (11%), $(Me_3Si)_2SiMe_2$ (12%), and IV (73%). All these products were identified by ^{1}H-NMR and mass spectroscopy. The NMR and mass spectral data are given in Table 2.

Photolysis of $MeSi(SiMe_3)_3$ in the presence of methanol. 2.0 g (7.6 mmol) of I, 0.97 g (3.0×10 mmol) of CH_3OH and 7 m*l* of cyclohexane were placed in the cylindrical quartz vessel. The reaction mixture was thoroughly degassed three times by the freeze-pump-thaw method. The sample was irradiated for 50 hr by medium-pressure mercury lamps. 50% of the starting material was consumed. The excess solvent was removed by a simple distillation. Final purification of the products was achieved by gas chromatography. The products obtained were $Me_3SiSiMe_3$ (65%), V (33%), $(Me_3Si)_2Si$-HME (11%), $(Me_3Si)_2SiMe_2$ (9.4%), and VI (19%).[18] All these products were identified by ^{1}H-NMR and mass spectroscopy. The spectroscopic properties of the product compounds are given in Table 2.

Photolysis of $MeSi(SiMe_3)_3$ in the presence of methanol-d_1 (CH_3OD). 2.0 g (7.6 mmol) of I, 1.0 g (3.0×10 mmol) of CH_3OD and 7 m*l* cyclohexane were placed in the cylindrical quartz vessel. The reaction mixture was thoroughly degassed three times by the freeze-pump-thaw method. The sample was irradiated for 70 hr by medium-pressure mercury lamps. 69% of the starting material was consumed. The excess solvent was removed by a simple distillation. Final purification of the products was achieved by gas chromatography. The products obtained were $Me_3SiSiMe_3$ (94%), V-d (48%), $(Me_3$-$Si)_2SiDMe$ (16%), $(Me_3Si)_2SiMe_2$ (6.4%), and VI-d_2 (12%). All these products were identified by ^{1}H-NMR and mass spectroscopy. The spectroscopic properties of the product compounds are given in Table 2.

Photolysis of $MeSi(SiMe_3)_3$ in the presence of triethylsilane. 2.0 g (7.6 mmol) of I, 2.7 g (23 mmol) of triethylsilane and 5 m*l* cyclohexane were placed in the cylindrical quartz vessel. The reaction mixture was thoroughly degassed three times by the freeze-pump-thaw method. The sample was irradiated for 60 hr by medium-pressure mercury lamps. 89% of the starting material was consumed. The excess solvent was removed by a simple distillation. Final purification of the products was achieved by gas chromatography. The products obtained were Me_3SiSMe_3 (70%), $(Me_3Si)_2SiHMe$ (3.4 %), $(Me_3Si)_2SiMe_2$ (1.7%), $EtSiSiH_2Me$ (1.5%), $Et_3SiSiHMe_2$ (0.4%), $Me_3SiSiEt_3$ (2.7%), $Et_3SiSiHMe(SiMe_3)$ (36%) and Et_3-$SiSiEt_3$ (0.5%). All these products were identified by ^{1}H-NMR and mass spectroscopy. The spectroscopic properties of the product compounds are given in Table 2.

Calculation. The calculations were performed using the PM3 methods as implemented in the MOPAC 6.0 package.[13] A microvax computer at the College of Natural Science of Chungnam National University was used for these PM3 calculations.

Results and Discussion

Since the UV absorption spectrum of I in a 5×10^{-4} M cyclohexane solution exhibits two maxima of $\lambda_{max}=230$ and 277 nm, we employed medium-pressure mercury lamps emitting mostly 254 nm wavelength.

When I was photolyzed using UV-light in a cyclohexane solution in the absence of trapping agents, only two stable products, $Me_3SiSiMe_3$ and $(Me_3Si)_2SiMe_2$ were observed.

$$I \xrightarrow[\text{cyclohexane}]{h\nu,\ 70\ \text{hr}} \underset{\text{II}}{Me\text{-}\ddot{S}i\text{-}SiMe_3} + Me_3SiSiMe_3 - 66.0\ \text{kcal} \quad (1)$$

$$\rightarrow \underset{50\%}{:SiMe_2} + \underset{8.7\%}{Me_2Si(SiMe_3)_2} - 62\ \text{kcal} \quad (2)$$

It is noted that all the reported yields in this paper are based on the amount of the unrecovered starting material, and the energetics reported in this paper is based on the experimental and/or theoretical (if the experimental data are not available) values of the enthalpies of formation given in Table 1.

These products have previously been observed in the recent study[11] and occur by reductive elimination: chain abridgement concomitant with extrusion of silylene II (process 1) and chain scission followed by a Me-shift with simultaneous loss of : $SiMe_2$ (process 2). Process 1 involving loss of the internal silicon atom is much more efficient than reaction 2 arising from the competing loss of the terminal silicon atom although process 1 is more endothermic than reaction 2. This low reaction efficiency may arise from a high energy barrier for a Me-Shift in process 2. A previous theoretical study[19] showed that the Me-shift concomitant with the formation of Me_2Si: involves a high energy barrier.

$$Me_3SiSiMe_3 \rightarrow Me_2Si: + SiMe_4 - 58\ \text{kcal} \quad (3)$$

$$\text{Log } A = 13.70 \pm 0.70,\ E_a = 67.14 \pm 0.76\ \text{kcal/mol}$$

This activation energy is calculated to be 9 kcal/mol in excess of the overall endothermicity of reaction 3.

When I was photolyzed in the presence of a two-fold excess of 2-methyl-1,3-butadiene, 1,3-dimethyl-1-(trimethylsilyl)-1-silacyclopent-3-ene (IV) is observed as the major product, along with Me_3SiSMe_3 and $Me_2Si(SiMe_3)_2$ and an unexpected product of $(Me_3Si)_2HMe$.

It is invoked that $HSiMe(SiMe_3)_2$ arises from silyl radical III *via* acquisition of a H-atom from 2-methyl-1,3-butadiene since the product is not observed in the neat photolysis. This observation is consistent with that of Davidson *et al.*[11] but contrasted with that of Karatsu *et al.*[7] who has observed that primary radicals formed in the homolytic cleavage of polysilanes $-(R_2Si)_n-$(R = hexyl) undergo a radical disproportionation.

An addition of Me_2Si: to the diene substrate has not been

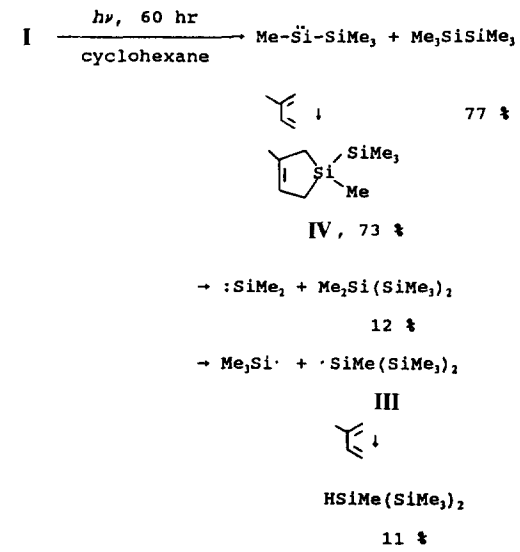

Scheme 2.

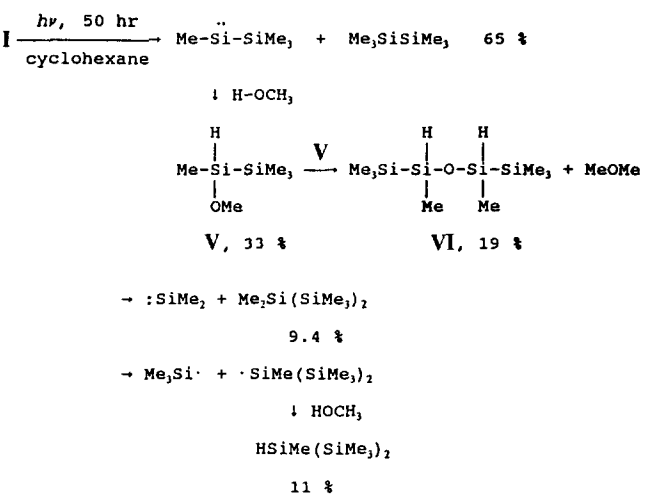

Scheme 3.

observed in that trapping experiment since the yield of the adduct may be under our gas chromatographic detection limit. But the silylene is identified by trapping with triethylsilane. This is detailed below.

Product IV is formed in a comparatively large yield since the product is likely to be quite stable upon the UV irradiation, and the addition to 2-methyl-1,3-butadiene is exothermic and efficient.[3,4]

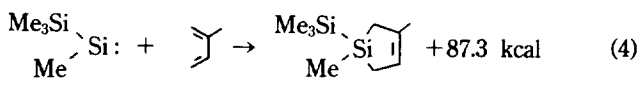

Formation of $HSiMe(SiMe_3)_2$ could be accounted for *via* H-abstraction from 2-methyl-1,3-butadiene by silyl radical III, process 5.

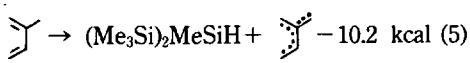

If a C_5H_7 radical with a structure shown in process 5 is involved in the intermolecular H-shift, silyl radical III remains in an vibrationally and/or electronically excited state due to process 6 since reaction 5 is endothermic.

$$MeSi(SiMe_3)_3 \rightarrow Me_3Si\cdot + \cdot SiMe(SiMe_3)_2 - 69.0 \text{ kcal} \quad (6)$$

Process 5 is energetically possible in this photolytic system since the 254 nm photon corresponds to 113 kcal/mol and only 69.0 kcal is necessitated in the homolytic cleavage, process 6. Or another photoabsorption of radical III could initiate process 5. The thermochemical data given in process 5 is determined by assuming that the radical shown in process 5 has a minimum energy among all possible structures with the chemical formula of C_5H_7.

Silyl radical III is also implicated by the isolation of $HSiMe(SiMe_3)_2$. Process 7 could account for its formation.

$$(Me_3Si)_2MeSi\cdot + HOMe \rightarrow (Me_3Si)_2MeSiH + \cdot OMe - 19.7 \text{ kcal} \quad (7)$$

We also observe one interesting product 1,1,1,2,4,5,5,5-octamethyltetrasiloxane (VI) whose formation seems puzzling, but apparently arises from a coupling of two molecules of 1-methoxy-1,2,2,2-tetramethyldisilane (V) with simultaneous extrusion of one molecule of dimethyl ether as shown below in Scheme 3. This is further discussed below.

The occurrence of process 7 strongly indicates that silyl radical III formed in process 7 lies in the vibrationally and/or electronically excited state. Actually VI is always observed in appreciable yields in the trapping systems employing methanol, ethanol and prop-2-en-1-ol.[20] Process 8 is likely to be involved in the formation of VI although the reaction mechanism for the formation of VI is not evidenced so far.

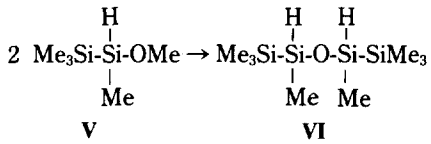

The coupling reaction seems to be favorable since the reaction is almost thermoneutral. Even though reaction 8 may involve a high activation energy, the reaction is possible since at least 77.2 kcal/mol is left in the internal energy *via* process 9.

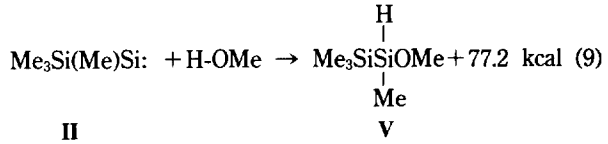

To clarify the coupling mechanism, it is necessitated to observe dimethyl and diethyl ethers as the counterparts of product VI. Note that we were actually indifferent to the ether products since quite recently product VI was identified and the mechanism for the formation of VI is elucidated. Failure to observe the ethers has prompted us to examine another trapping experiment employing prop-2-en-1-ol in the hope that bis(2-propenyl) ether is easily isolated since the ether is less volatile than dimethyl and diethyl ether. In the prop-2-en-1-ol system, bis(2-propenyl) ether and its counterpart VI are observed.[21] The similar coupling reaction, process 10 could account for the photodissociation.

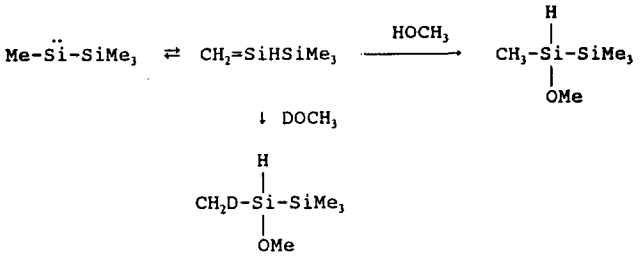

Scheme 4.

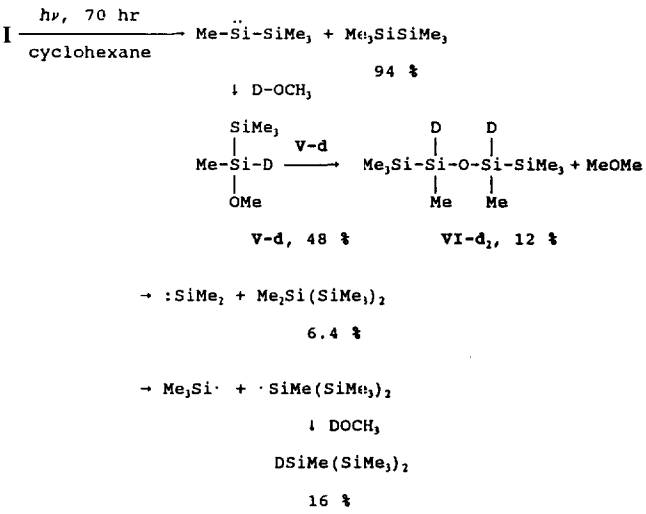

Scheme 5.

$$2\ Me_3Si\text{-}\underset{\underset{Me}{|}}{\overset{\overset{H}{|}}{Si}}\text{-}O\text{-}CH_2\text{-}CH{=}CH_2 \rightarrow Me_3Si\text{-}\underset{\underset{Me}{|}}{\overset{\overset{H}{|}}{Si}}\text{-}O\text{-}\underset{\underset{Me}{|}}{\overset{\overset{H}{|}}{Si}}\text{-}SiMe_3 + CH_2{=}CH\text{-}CH_2\text{-}O\text{-}CH_2\text{-}CH{=}CH_2 \quad (10)$$

VIII **VI**

It is interesting to deduce the source of the H-atoms in $HSiMe(SiMe_3)_2$ and VI and to infer the reaction mechanism for formation of V since V can be formed *via* the insertion of silylene II into H-OCH_3 as shown in Scheme 3 or by a silylene-to-silene rearrangement followed by oxidative addition of methanol to the silene, as shown in Scheme 4.

Labelling experiment employing a partially deuteriated methanol of CH_3OD is quite informative as to these matters.

When I was photolyzed in the presence of a 3.9-fold excess CH_3OD under the similar conditions for the CH_3OH reaction system, instead of $HSiMe(SiMe_3)_2$, $DSiMe(SiMe_3)_2$ is observed as the exclusive product as outlined in Scheme 5.

In an attempt to trap Me_2Si: being formed photochemically from I, a trapping experiment employing triethylsilane was performed. When I was photolyzed in the presence of a 3.1-fold excess of triethylsilane, the insertion of dimethylsilylene into triethylsilane is observed as a minor pathway, process 11.

$$Me_2Si: + H\text{-}SiEt_3 \rightarrow HMe_2SiSiEt_3\ (0.4\%) \quad (11)$$

The other products are accounted for by the primary silylene insertion reactions and/or the secondary photochemical

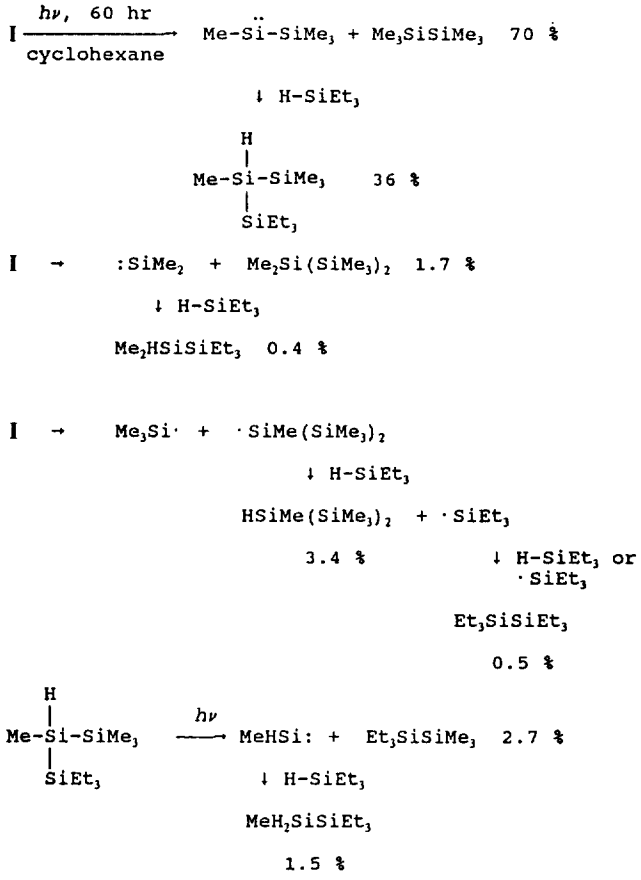

Scheme 6.

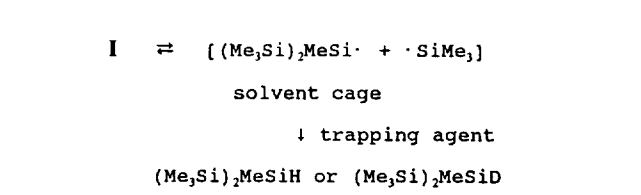

Scheme 7.

reactions of the primary products.

As seen in the neat photolytic system, the apparent photochemical dissociation of I is only 28%, the value being much smaller than in the trapping systems, and the total yield of the volatile products is only 58.7%, being much smaller collection efficiency of the stable products. Without trapping agents, the photolytic decomposition of I is very inefficient presumably due to the reversibility of the homolytic cleavage in the solvent cage as shown in Scheme 7.

Actually, in the trapping experiments employing various alcohols of methanol, ethanol and prop-2-en-1-ol, the degradation of I is 50% for methanol, 41% for ethanol, 90% for prop-2-en-1-ol and 89% for triethylsilane due probably to the facile radical scavenging by the trapping agents.[22]

Acknowledgments. This work was financially supported by the Ministry of Education, Korea (a non-directed fund of 1988-1990) and also partially supported by the Basic Science Research Institute Program (1992-1993), the Ministry of Education, Korea, and by the Korea Science and Engineering Foundation.

References

1. Miller, R. D.; Michl, J. *J. Chem. Rev.* **1989**, *89*, 139.
2. Ishikawa, M.; Kumada, M. *Revs. Si, Sn and Pb Compounds* **1979**, *IV*, 7.
3. Gaspar, P. P.; Holten, D.; Konieczny, S.; Corey, J. Y. *Acc. Chem. Res.* **1987**, *20*, 329.
4. Gaspar, P. P.; Boo, B. H.; Chari, S.; Ghosh, A. K.; Holten, D.; Kirmaier, C.; Konieczny, S. *Chem. Phys. Lett.* **1984**, *105*, 153.
5. Ishikawa, M.; Kumada, M. *J. Organomet. Chem.* **1972**, *42*, 325.
6. Ishikawa, M.; Takaoka, T.; Kumada, M. *J. Organomet. Chem.* **1972**, *42*, 333.
7. Karatsu, T.; Miller, R. D.; Sooriyakumaran, R.; Michl, J. *J. Am. Chem. Soc.* **1989**, *111*, 1140.
8. McKinley, A. J.; Karatsu, T.; Wallraff, G. M.; Miller, R. D.; Sooriyakumararan, R.; Michl, J. *Organometallics* **1988**, *7*, 2567.
9. McKinley, A. J.; Karatsu, T.; Wallraff, G. M.; Thompson, D. P.; Miller, R. D.; Michl, J. *J. Am. Chem. Soc.* **1991**, *113*, 2003.
10. Ishikawa, M.; Kumada, M. *J. Chem. Soc. D.* **1971**, 489.
11. Davidson, I. M. T.; Michl, J.; Simpson, T. *Organometallics* **1991**, *10*, 842.
12. Stewart, J. J. P. *J. Comp. Chem.* **1989**, *10*, 221.
13. Coolidge, M. B.; Stewart, J. J. P. *OCPE Program No. 455.*
14. Dewar, M. J. S.; Zoebisch, E. G.; Healy, E. F.; Stewart, J. J. P. *J. Am. Chem. Soc.* **1985**, *107*, 3902.
15. Dewar, M. J. S.; Jie, C. *Organometallics* **1987**, *6*, 1486.
16. The product mixtures in all these reaction systems were purified under the same gas chromatographic condition.
17. Barton, T. J. unpublished results. Also the synthetic procedure can be found in: Boo, B. H. The Chemistry of Silylsilylenes: Generation and Reactions of Trimethylsilylsilylene and Silylsilylene, Doctoral dissertation, Washington University, St. Louis, 1984.
18. Since one molecule of VI contains two subunits of silylene II, the yields of VI and VI-d_2 reported here is corrected to be twice larger than the measured yield based on the amount of the unrecovered starting material.
19. Davidson, I. M. T.; Howard, A. V. *J. Cheml. Soc., Faraday Trans. I*, **1975**, *71*, 69.
20. The photolysis of I in the presence of ethanol and 2-prop-2-en-1-ol is under study in our laboratory.
21. Only the mass spectrum is obtained since a tiny amount of the product is formed; mass: M^+ 98 (5.7), 84 (71), 83 (18), 69 (30), 56 (100), 55 (55), 44 (13), 43 (15), 42 (28), 41 (75), 39 (32), 32 (24).
22. It should be noted that the % decompositions do not exactly correspond to the scavenging efficiencies of the reactive silicon species since the UV irradiation time and the mole ratios of the reaction mixtures little differ each other.

A Quantitative Determination of Overlapped Chromatographic Peaks of Dysprosium and Yttrium Using Target Transformation Factor Analysis

Joon Myong Song, Chul Lee*, and Koo Soon Chung

Department of Chemistry, Sogang University, Seoul 121-742
**Department of Chemistry, Hanyang University, Seoul 133-791*
Received September 10, 1993

Rare earth elements (REE) were individual separated by applying the gradient elution *via* HPLC using α-hydroxy isobutyric acid (HIBA) as an eluent. However, the overlap of Y and Dy peaks was too severe to obtain the resolution of these two peaks. The target transformation factor analysis (TTFA) was applied to resolve the elution peaks of Y and Dy. $[A]_{raw}$ formed from the absorbances of mixed solution was factor analyzed. The abstract factor analysis (AFA) was used to determine the number of components that contributed to the poorly resolved peaks. The error theory in the AFA showed that the number of components was 2. The test vectors which correspond to pure component were selected from the standard solutions of Y and Dy. TTFA was accomplished by target testing. The results showed that the resolution of two peaks as well as the determination of Y and Dy were possible by the factor analysis.

Introduction

The utilization of high performance liquid chromatography (HPLC) procedures for the separation and determination of rare earth elements (REE) was well documented.[1] The REE were usually separated using a concentration gradient of eluting agent. However, because of close similarity in their chemical properties, the resolutions of HPLC for the separation of individual REE were difficult to achieve. For example, the gradient elution by HPLC was applied to separate individual REE using α-hydroxy isobutyric acid (HIBA) as an eluent. However, the overlap of the Y and Dy was too severe